Build Simul (2023) 16: 2343–2361
https://doi.org/10.1007/s12273-023-1011-7

Comfort assessment and energy performance analysis of a novel adjustable semi-transparent photovoltaic window under different rule-based controls

Yutong Tan[1,2], Jinqing Peng[1,2] (✉), Meng Wang[3], Yimo Luo[1,2], Aotian Song[4], Nianping Li[1,2]

1. College of Civil Engineering, Hunan University, Changsha, Hunan, China
2. Key Laboratory of Building Safety and Energy Efficiency of the Ministry of Education, Changsha, Hunan, China
3. School of Energy and Power Engineering, Changsha University of Science and Technology, Changsha, Hunan, China
4. Leadus Glass Technology (shenzhen) Co., LTD, Shenzhen, Guangzhou, China

Abstract

Self-powered photovoltaic windows, which integrate photovoltaic with electrochromic devices, have attracted widespread attention of scholars since they can generate electricity in situ and reduce building energy consumption by modulating the transmitted solar radiation. However, previous studies mainly focused on the material development and performance characterization, lack of comfort assessment and energy saving potential of its application to buildings. To address this issue, an adjustable semi-transparent photovoltaic (ATPV) window which integrates CdTe-based photovoltaic and WO_3-based electrochromic, was taken as the research object, and a novel rule-based control strategy taking the beam solar radiation luminous efficacy (CtrlEff) as decision variable was proposed for the first time. The ATPV window model was established in WINDOW software based on the measured data, and then it was exported to integrated with a medium office building model in EnergyPlus for performance evaluation including the visual comfort, thermal comfort, net energy consumption, and net-zero energy ratio. The results of a case study in Changsha (E 112°, N 28°) indicated that the ATPV window under the CtrlEff strategy can effectively reduce the southward and westward intolerable glare by 86.9% and 94.9%, respectively, and increase the thermal comfort hours by 5% and 2%, compared to the Low-E window. Furthermore, the net-zero energy consumption can be decreased by 58.7%, 65.7%, 64.1%, and 53.8% for south, west, east, and north orientations, and the corresponding net-zero energy ratios are 65.1%, 54.6%, 62.7%, and 61.6%, respectively. The findings of this study provide new strategies for the control and optimization of the adjustable window.

Keywords

adjustable semi-transparent photovoltaic windows;
rule-based control;
visual comfort;
energy consumption;
net-zero energy ratio

Article History

Received: 13 December 2022
Revised: 05 February 2023
Accepted: 20 February 2023

1 Introduction

The building operation energy usage in China accounts for 21% of China's total primary energy consumption (Hu et al. 2022). Building exterior windows, which play an indispensable role in the interactions between the indoor and outdoor environments for occupants, constitute one of the weakest components of building envelopes and lead to a majority of energy consumption used to maintain the thermal and visual comfort of occupants for lighting, heating, and cooling. Recent efficient windows, like the low-emissivity window (Urbikain 2020), aerogel window (Zhang et al. 2021), and vacuum window (Fang et al. 2020), were developed with a better thermal insulation performance, but are unable to solve the problem of changing energy demand with transient meteorological boundary conditions. Hence, adjustable smart windows, which can respond to external stimuli or occupants' needs, are increasingly attracting widespread attention (Zhou et al. 2021; Castillo et al. 2022).

Smart windows can be grouped into passive and active technologies. Passive technologies include thermotropic (TT) (Yao and Zhu 2012), thermochromic (TC) (Aburas et al.

E-mail: jqpeng@hnu.edu.cn

List of symbols

ATPV	adjustable semi-transparent photovoltaic window	PCE	photon-to-electron conversion efficiency
CtrlEff	beam solar radiation luminous efficacy control	PMV	predicted mean vote
CtrlHeat	heat flow control	R_g	glare reduction (%)
CtrlIll	indoor illuminance control	R_{net}	ratio of net-zero energy hours (%)
CtrlRad	incident solar radiation control	R_{sol}	solar reflectance
DGI	discomfort glare index	SHGC	solar heat gain coefficient
EMS	energy management system	T_{sol}	solar transmittance
I_t	thermal performance improvement (%)	T_{vis}	visible transmittance

2019; Hong et al. 2021), photochromic (PC) (Al-Qahtani et al. 2022), and phase change material (PCM) (Huang et al. 2023) glazing with a self-triggered mechanism, while active technologies are mainly electrically activated such as suspended particle devices (SPD) (Ghosh and Norton 2019) and polymer dispersed liquid crystal (PDLC) (Ghosh et al. 2018) triggered by alternative current voltage and electrochromic (EC) rely on direct current voltage (Zhao et al. 2018). Among various smart windows, EC windows were reported to have the greatest development prospects in future buildings since their thermal and visual properties can be actively adjusted by applying a small voltage (Jelle et al. 2012). The tint states of the EC window can be modulated to utilize the solar heat in winter and reject the undesired heat gain in summer. It has been reported that EC windows with illuminance control strategy can reduce 14% annual energy consumption in Rome, Italy (Baldassarri et al. 2016). With MPC control, the annual energy consumption of a single office room can be reduced up to 37% in Mannheim, Germany (Ganji et al. 2021). Based on the superior energy efficiency of EC windows, researchers are dedicated to realizing the net-zero energy goal by integrating renewable energy like photovoltaic (PV) technology, which represents an innovative and cost-effective measure as the energy sector transition towards carbon neutrality (Balta-Ozkan et al. 2021). PV technology is a proven technology for harnessing renewable solar energy, and PV windows in modern highly-glazed buildings have been attracting widespread attention of scholars. The integration of EC and PV technologies has two main advantages: (1) responding to changes of the outdoor environment to reduce peak loads and annual energy consumption while ensuring indoor comfort; (2) harnessing solar radiation to generate electricity in situ and reducing the dependence on the utility grid. In general, there are three different approaches to combine the above two technologies: (i) stand-alone side-by-side (SS), (ii) monolithically integrated (MN), and (iii) photoelctrochromic device (PECD) (Deb et al. 2001). The SS structure means that the PV cells and EC coating are deposited on separate glasses, and then the two glasses are combined. The MN structure indicates that PV and EC are deposited on the same glass. The PECD is based on the photovoltachromic cell, which is able to take solar energy to stimulate chromic behavior with the characteristic of tunable transmittance (Wu et al. 2009). Recent efforts on the above windows have been reviewed and concluded in Table 1. It is seen that different types of PV cells, perovskite, dye-sensitized solar cells (DSSC), and amorphous silicon (a-Si) cells, have been used for developing PVEC devices with fast respond time and widespread optical modulation. It is seen that the power conversion efficiency (PCE) of the PVEC window with DSSC cells (around 2%) is much lower than that with perovskite cells (up to 20.5%). Compare the characteristics of the PVEC windows with perovskite cells,

Table 1 Summary of the recently windows combining PV and EC technologies

Reference	Size (cm×cm)	Cell	PCE (%)	Respond time (s)		Optical modulation	Stability loss of ΔT/cycles
				Coloring	Bleaching		
Ling et al. 2022	5×5.4	Perovskite	20.5	2	5	70%	13.4%/70000 cycs
Ling et al. 2021	n.a.	Perovskite	18.3	2.7	27.6	71%	1.1%/60000 cycs
Xia et al. 2016	n.a.	Perovskite	n.a.	2.5	2.6	43%	n.a.
Cheng et al. 2021	2×3	DSSC	2.2	5.5	3.3	31%	n.a.
Wang et al. 2021	20×20	n.a.	n.a.	14	250	40%	8%/450 cycs
Fiorito et al. 2020	n.a.	DSSC	1.84	n.a.	n.a.	31.5%	n.a.
Huang et al. 2012	n.a.	a-Si	9.44	30	15	70%	n.a.

the window with faster bleaching time shows a worse stability. Though the characteristics of the PVEC window have been studied and are being enhanced, their performance of applying to buildings lacks of in-depth analysis since most of the above windows were stayed at the laboratory stage with a small size.

As reported, the energy benefits of adjustable windows depend not only on their optical and thermal properties but also on climatic conditions and control strategies simultaneously (Favoino et al. 2015). Researchers (Yik and Bojić 2006) found that the application of EC windows could lead to a reduction of the annual cooling energy by up to 6.6% in high-rise residential buildings located at low latitudes (Hong Kong). While in high latitude cities, such as Helsinki, EC windows don't bring any energy benefits compared to conventional static windows (Pal et al. 2016). Additionally, different control strategies of the EC windows lead to an obvious discrepancy in energy savings and comfort, and the strategies can be grouped into two categories: (i) rule-based controls and (ii) optimized controls (Krarti et al. 2022). Most of the existing researches on smart windows adopted rule-based controls based on solar radiation (Gugliermetti and Bisegna 2003; Assimakopoulos et al. 2007; Jonsson and Roos 2010; Tavares et al. 2014; Oh et al. 2018; Piccolo et al. 2018; Fiorito et al. 2020), illuminance (Sullivan et al. 1994; Assimakopoulos et al. 2007; Fernandes et al. 2013; Gonzalez and Fiorito 2015; Ritter et al. 2015), outdoor air temperature (Gonzalez and Fiorito 2015; Fathi and Kavoosi 2021), indoor air temperature (Ritter et al. 2015; Scorpio et al. 2020), heating/cooling load (Jonsson and Roos 2010), occupancy (Assimakopoulos et al. 2007; Jonsson and Roos 2010), and thermal comfort indicator (Khatibi et al. 2022). Among these, solar radiation is the most widely used decision variable for smart window controlling, and the threshold varies from 95 W/m^2 (Lee and Tavil 2007), 150 W/m^2 (Tavares et al. 2016), 200 W/m^2 (Jonsson and Roos 2010), 250 W/m^2 (Loonen and Hensen 2015), 350 W/m^2 (Assimakopoulos et al. 2007), to 850 W/m^2 (Gugliermetti and Bisegna 2003). However, Krarti (2022) indicated that the use of the thermal load as a decision variable offers the highest energy efficiency potential compared to solar radiation and temperature controls for commercial buildings in four US locations. A recent study in Iran showed that indoor air temperature control has the highest energy savings among the three controls of indoor air temperature, outdoor air temperature, and diffuse radiation (Fathi and Kavoosi 2021). In the above research, the most commonly used control strategy (radiation control) did not show the highest energy savings. This is because solar radiation-based control strategy focused on avoiding glare rather than avoiding unwanted heat flow. To minimize building energy consumption while maintaining indoor comfort, the model predictive control (MPC) is considered as one of the most promising strategies for adjustable windows (Serale et al. 2018). Ganji et al. (2021) indicated that an MPC for EC glazing save energy by up to 14%–37% for different orientations while providing visual and thermal comfort relative to a double-pane window. Though the control effect of MPC is more efficient compared to rule-based controls, its high requirements on the underlying model and prediction speed limit the wide application. Therefore, the rule-based control is the mainstream in practical applications.

In summary, researchers have pointed out that the integration of PV and EC technologies on windows is expected to stimulate significant energy-saving effects and maintain a comfortable indoor environment, and the corresponding materials have been developed with obvious optical modulation and fast coloration. However, there are several problems remain unsolved: 1) the energy performance of the PV integrated electrochromic window at the building level has not been studied thoroughly, (2) the suitable decision variables and control strategies for this window are ambiguous, and (3) a comprehensive evaluation that considers the contradictory conflicts between comfort and energy saving has not been investigated. To address the above issues, this study established a side-by-side adjustable semi-transparent (ATPV) window and proposed a novel control strategy using the beam radiation luminous efficacy as the decision variable (CtrlEff). Based on this, the comprehensive performance of the ATPV window under the CtrlEff strategy, including visual comfort, thermal comfort, net energy consumption and the net-zero energy ratio, were analyzed and compared with other commonly used rule-based control strategies. The rest of this paper is structured as follows: first, the overview of the research framework was introduced in Section 2.1, and then the configuration of the ATPV window and the parameter settings of the building model was given in Section 2.2 and Section 2.3. The control strategies were determined in Section 2.4, and the selected evaluation metrics were listed in Section 2.5. Through the simulation conducted in EnergyPlus, the performance of the ATPV window was analyzed in Section 3. Finally, the main conclusions of this study were drawn in Section 4.

2 Research methodology

2.1 Overview of the research framework

The research framework of this study is shown in Figure 1. Firstly, the models of the ATPV window and the comparison windows were established based on the measured data. Then, a building model with a core zone and four perimeter zones, derived from the US Department of Energy's (DOE)

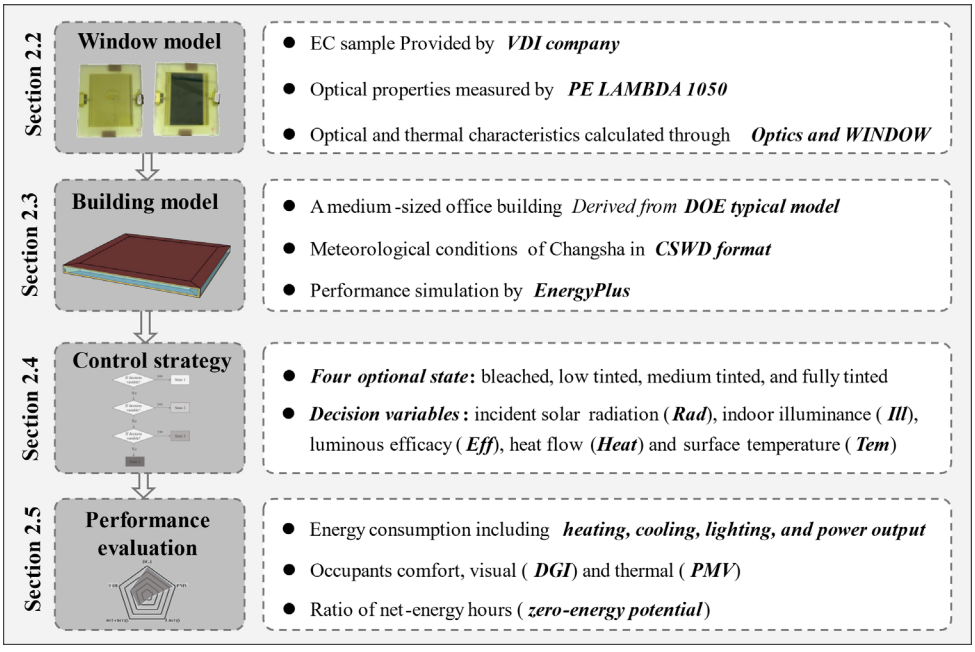

Fig. 1 Research framework

typical medium office model, was modeled in EnergyPlus. To develop a suitable control strategy, the correlations between several measurable parameters and visual comfort were analyzed, and the parameters with the highest correlation degree were selected as the decision variables. Further, the metrics for comprehensive evaluation of the performance of the ATPV window under different control strategies were introduced, including energy consumption, daylight glare index (DGI), predicted mean vote (PMV), and the ratio of net-zero energy hours.

2.2 Configuration of the ATPV window

As reviewed in Section 1, photovoltaic and electrochromic technologies can be integrated through three ways, namely side-by-side, monolithically integrated, and photovolchromic devices. In this study, the side-by-side construction was adopted to establish the ATPV window due to the maturity of current technology and material limitations. As depicted in Figure 2, the PV and EC laminate glass are made separately and then combined with a cavity which is filled with a mixed gas of 10% air and 90% argon. The semi- transparent PV glazing was placed at the exterior part of the ATPV window to maximize the utilization of incident solar radiation, and the tunable EC glazing arranged at the interior part was used to adjust the tint states of the window for glare and overheating protection. Besides, the mixed inert gas filled in the cavity between the above two glazing was used to improve the thermal performance of the window.

The tunable EC laminate located at the interior part of the ATPV was provided by the VDI Glass company with four pre-set adjustable gears, and its tint states can be adjusted with the applied voltages of 0 V, 0.5 V, 1.0 V, and 1.8 V. The corresponding spectral optical properties were measured through a spectrophotometer, PE LAMBDA 1050. As depicted in Figure 3, it is seen that the EC laminate is a conventional one since both the visible and near-infrared transmittance decrease as the applied voltage increases. Figure 3(a) shows the tint states of the EC sample under different applied voltages, and the spectral transmittance and reflectance are shown in Figures 3(b) and (c). The visible transmittance (T_{vis}) of the EC sample is calculated by the following expression (Granqvist et al. 2007):

$$T_{vis} = \frac{\sum_{380\,nm}^{780\,nm} T(\lambda) D_\lambda V(\lambda) \Delta\lambda}{\sum_{300\,nm}^{2500\,nm} D_\lambda V(\lambda) \Delta\lambda}$$

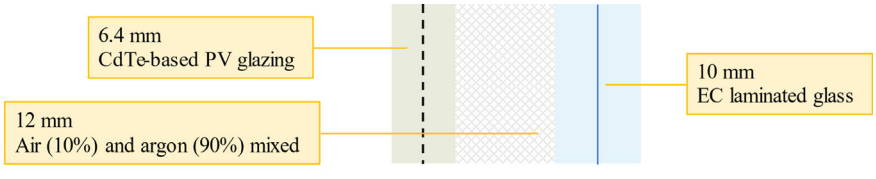

Fig. 2 Sectional view of the side-by-side ATPV window

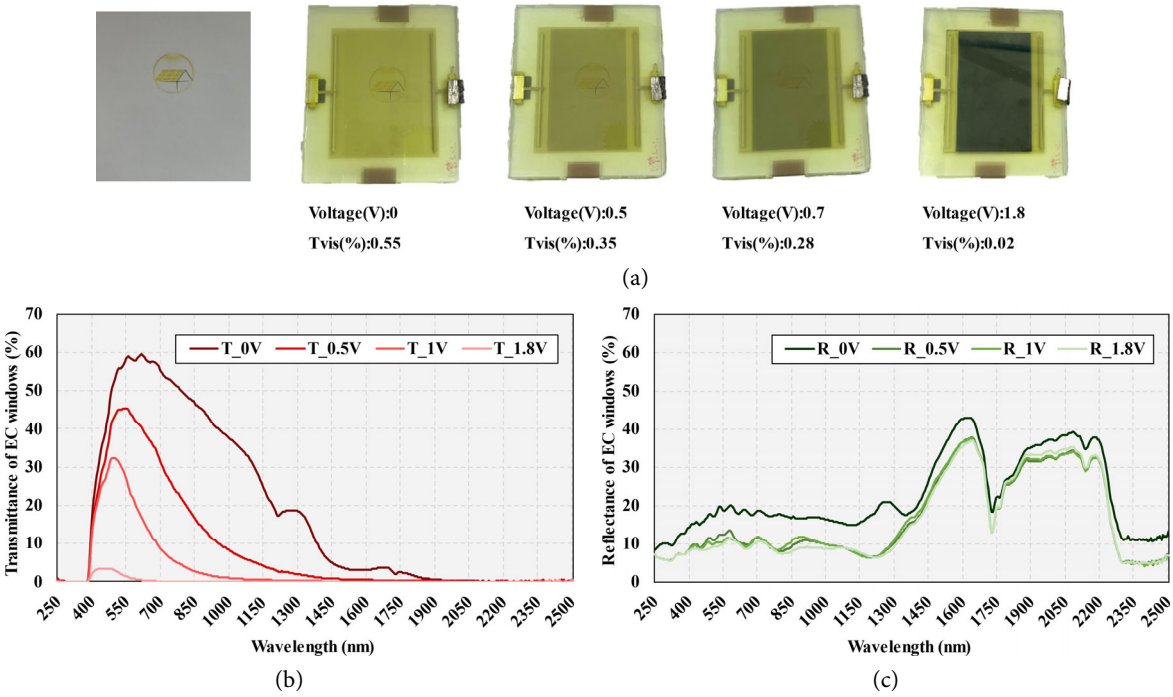

Fig. 3 (a) EC laminate under different voltages, (b) spectral transmittance, and (c) spectral reflectance

where D_λ is the relative spectral distribution of illuminant D65, $T(\lambda)$ is the spectral transmittance of the EC sample at the give wavelength, $V(\lambda)$ is the spectral luminous efficiency for photopic vision of a standard observer, and $\Delta\lambda$ is the wavelength interval. Considering the contribution of infra-red radiation, the solar transmittance (T_{sol}) and solar reflectance (R_{sol}) are given by the following equations:

$$T_{sol} = \frac{\sum_{300\,nm}^{2500\,nm} T(\lambda) S_\lambda \Delta\lambda}{\sum_{300\,nm}^{2500\,nm} S_\lambda \Delta\lambda}$$

$$R_{sol} = \frac{\sum_{300\,nm}^{2500\,nm} R(\lambda) S_\lambda \Delta\lambda}{\sum_{300\,nm}^{2500\,nm} S_\lambda \Delta\lambda}$$

where S_λ is the relative spectral distribution of solar radiation. Under the applied voltage of 0 V, 0.5 V, 1.0 V and 1.8 V, the corresponding average visible transmittance of the EC laminate are 55%, 35%, 19% and 2%, and the solar reflectance are 19%, 12%, 12% and 10%, respectively.

As for the exterior CdTe-based semi-transparent PV laminate glass, its optical properties are closely related to the solar cell coverage rate, and in this study, the PV laminate glass with a coverage rate of 40% was adopted. The spectral optical properties of the PV laminate were also measured by the spectrophotometer, shown in Figure 4, and then imported to the Optics program together with that of the EC laminate. Further, the ATPV window models with different tint states were established in WINDOW software, and the optical and thermal performances of the whole window

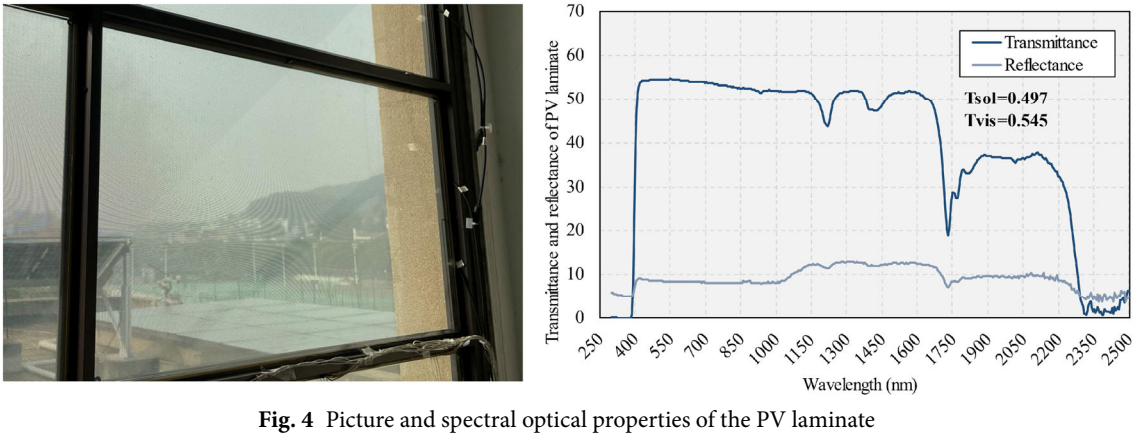

Fig. 4 Picture and spectral optical properties of the PV laminate

were characterized by *U*-value, solar heat gain coefficient (SHGC), and visible transmittance (T_{vis}). For an adjustable window, the *U*-value is fixed while the SHGC and T_{vis} change with the applied voltage. As listed in Table 2, the *U*-value of the ATPV window is fixed at 2.520 W/(m²·K) under different applied voltages, while the T_{vis} varies from 0.304 to 0.007. In addition to the ATPV window model, a double-pane window consisting of a piece of clear glass, a 12 mm argon gap, and a piece of Low-E glass, was also established in WINDOW for comparison. Detailed characteristics of both the ATPV window and the comparison window are listed in Table 2.

Table 2 Information on different windows used in this study

Name	States	Construction	*U*-value W/(m²·K)	SHGC	T_{vis}
ATPV_1	Bleached	PV laminate + 12 mm argon + EC laminate	2.520	0.418	0.304
ATPV_2	Low tinted			0.405	0.229
ATPV_3	Medium tinted			0.391	0.132
ATPV_4	Fully tinted			0.367	0.007
Low-E	Static	Clear glass + 12 mm argon + Low-E glass	1.563	0.587	0.524

2.3 Description of building model and locations

This study focused on office buildings, thus, the building model referred to the typical commercial buildings from the US Department of Energy firstly, and then some local adjustments were made to by combining the characteristics of the ATPV windows. As depicted in Figure 5, the middle layer of the medium-size office building was chosen as the building model, of which the ceiling, the floor, and the interior walls are assumed to be adiabatic. The total floor area of the building model is 1650 m², and it is divided into five thermal zones including a core zone and four perimeter zones. In order to fit more closely with the modern and popular glass curtain wall architecture, the window-to-wall ratio (WWR) of the building model was expanded to 70%, and each window can be controlled separately. The lighting system used in this study adopted a dimming control system, in which the power of the lamps changes with the difference between the pre-setting reference illuminance and the real-time measured illuminance. The reference points for the lighting control in each perimeter zone were set at 1.5 m, 2.5 m, and 3.5 m away from the window on the central axis at a height of 0.75 m. As for the HVAC system, a reversible heat pump was adopted to maintain the heating and cooling set temperature in air conditioning seasons. The PMV calculation is based on the Fanger's thermal comfort model, where, the temperature used for

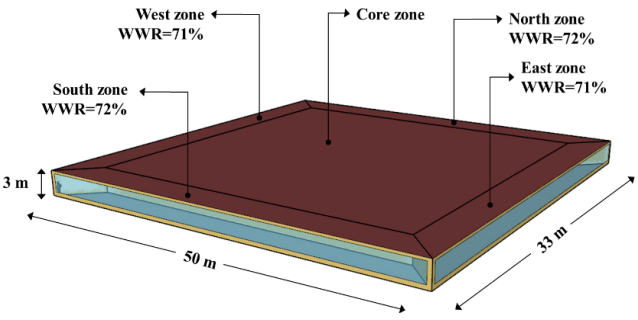

Fig. 5 3D model of the reference building

PMV calculated is the mean radiant temperature of the whole thermal zone, the clothing factors in summer and winter are set to 0.5 clo and 1.0 clo, the air velocity is set as 0.1 m/s, the metabolic rate during working hours is set as 1 met. The PV power generation model with temperature coefficient correction was adopted in this study to calculated the instantaneous PV electricity production. The PV coverage of the ATPV windows is 40%, and the energy conversion efficiency of the CdTe cells is 15% with the temperature coefficient of −0.25 %/°C. Detailed simulation settings in EnergyPlus are listed in Table 3. It is noting that the subsequent study focuses only on the four perimeter zones, since the energy consumption and visual comfort in the core zone is hardly affected by exterior windows.

2.4 The control strategies

The performance of the adjustable window is not only related to its optical and thermal characteristics, but also greatly influenced by control strategies. Commonly, the control strategy was developed to avoid discomfort glare. When occupants feel visually uncomfortable, they can dim the ATPV window to alleviate this discomfort. However, the prediction of glare is time-consuming and cost-intensive (Qiu et al. 2020). Besides, the camera used to capture the bright picture in office buildings caused privacy concerns for the occupants. Therefore, it is essential to find a detectable parameter with a high correlation with the glare indicator for the active control of the ATPV window. For this goal, a full-year simulation with the bleached state of the APTV window was performed initially, and the glare indicator, discomfort glare index (DGI), was obtained through the simulation. The correlations between DGI and hourly detectable parameters including diffuse solar radiation, direct solar radiation, exterior horizontal beam illuminance, exterior beam normal illuminance, diffuse solar radiation luminous efficacy, beam solar radiation luminous efficacy, sky brightness, incident solar radiation, incident beam solar radiation, and indoor illuminance are plotted in Figure 6. It is seen that the beam solar radiation luminous

Table 3 Specifications of the building model

Item	Description
Geometry	55 m in length, 33 m in depth, and 3 m in height Window area: 107.8 m^2 for south and north, 70.4 m^2 for west and east Window-to-wall ratio: 72% for south and north, 71% for west and east
Location	Changsha (E112°59′, N28°12′) Thermal region: hot summer and cold winter region Daylight region: the V daylight region (average annual illuminance of daylight is less than 30000 lx) Maximum temperature = 38.2 °C, minimum temperature = −3.2 °C
Roof and floor	Adiabatic
Wall construction	*U*-value of exterior wall = 0.58 W/(m^2·K) , other walls are adiabatic (MOHURD 2021)
Occupancy period	From 8 a.m. to 6. p.m. on week days, otherwise unoccupied
Internal gains (Dahanayake and Chow 2018)	People: 9 m^2/ person Equipment: 20 W/m^2
Infiltration	0.45 air change per hour
Lighting system	Power: 14 W/m^2 Efficiency: 80%
HVAC system	Cooling set point: 26 °C Heating set point: 20 °C (MOHURD 2020) Efficiency: a reversible heat pump with the efficiency of 4.0 for heating and 4.2 for cooling (MOHURD 2015)
HVAC seasons	Cooling season: 6.25–8.23; heating season: 12.26–2.11 (Chen et al. 2018; Tan et al. 2022)
Daylight model	Dimming to maintain 450 lx at the daylight reference point of each perimeter zone (MOHURD 2012) Daylight reference points are set at 1.5m, 2.5 m, and 3.5 m from the window on the central axis of each perimeter zone at a height of 0.75 m Glare reference point is set at 1 m from the window on the central axis of each perimeter zone with a height of 1.2 m
Thermal model	Fanger' PMV-PPD model Clothing factor (summer = 0.5 clo, winter = 1.0 clo) Metabolic rate = 1 met, air velocity = 0.1 m/s
PV model	Simple model: PV coverage = 40%, CdTe efficiency = 15%, temperature coefficient = −0.25%/°C

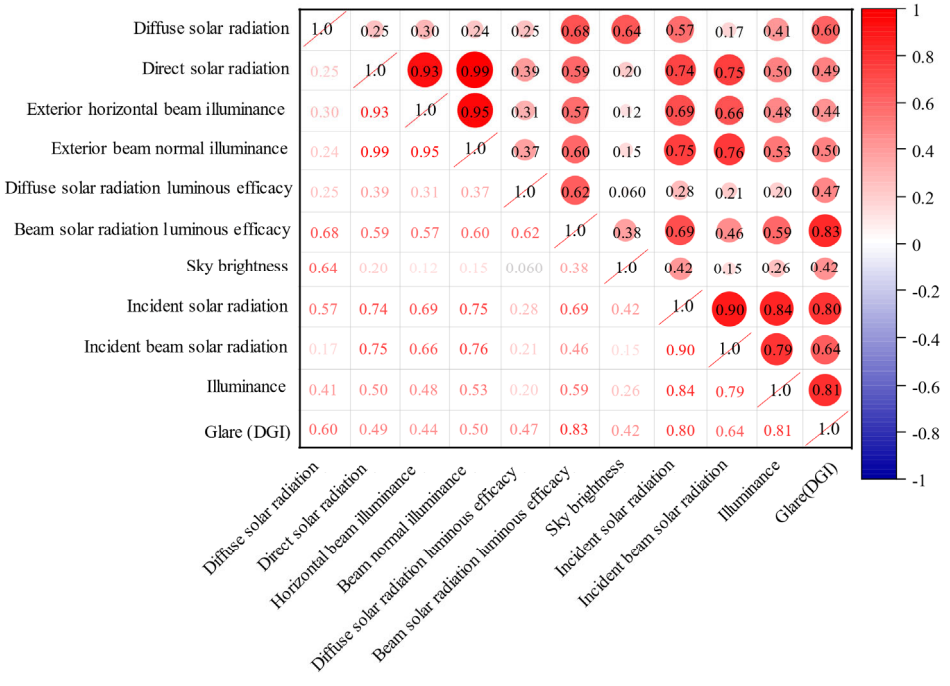

Fig. 6 The correlation coefficient graph among DGI and monitorable parameters

efficacy (defined as the ratio between illuminance and irradiance) (Eff), incident solar radiation (Rad), and indoor illuminance (Ill) have the highest correlation with DGI, therefore, the three parameters were adopted as decision variables to control the ATPV window for the purpose of glare protection.

As for the cities in the northern hemisphere, the east- and north-facing thermal zones receive relatively few solar radiation resources and cause less discomfort glare, thus only south and west orientations are considered for glare control using the above three decision variables. The control thresholds for each gear were determined by plotting the distribution of each decision variable against the DGI, as shown in Figure 7. The DGI was divided into four bins, namely imperceptible (DGI < 18), perceptible (18 < DGI < 24), disturbing (24 < DGI < 31), and intolerable (DGI > 31). The control goal is to keep the DGI below 18, and the detailed rules are listed in Table 4. Furthermore, the tint state of the ATPV window not only influences the visual comfort but also the energy consumption because SHGC varies with the tint states. For the energy-saving purpose, Krarti (2022) has compared the energy saving potential of the smart windows with different control strategies and indicated that the cooling and heating load control results in the highest energy saving rate. However, the monitoring of cooling and heating loads is relatively complicated in an actual project, thus, the heat flow through the window was considered instead in this study. The distribution of the heat flow through the ATPV window versus the hourly energy consumption is shown in Figure 8 and the detailed control rules are listed in Table 4.

According to the analysis above, four control strategies, namely incident radiation control (CtrlRad), indoor illuminance control (CtrlIll), beam solar radiation luminous efficacy control (CtrlEff), and heat flow control (CtrlHeat) were considered to evaluate the comprehensive performance

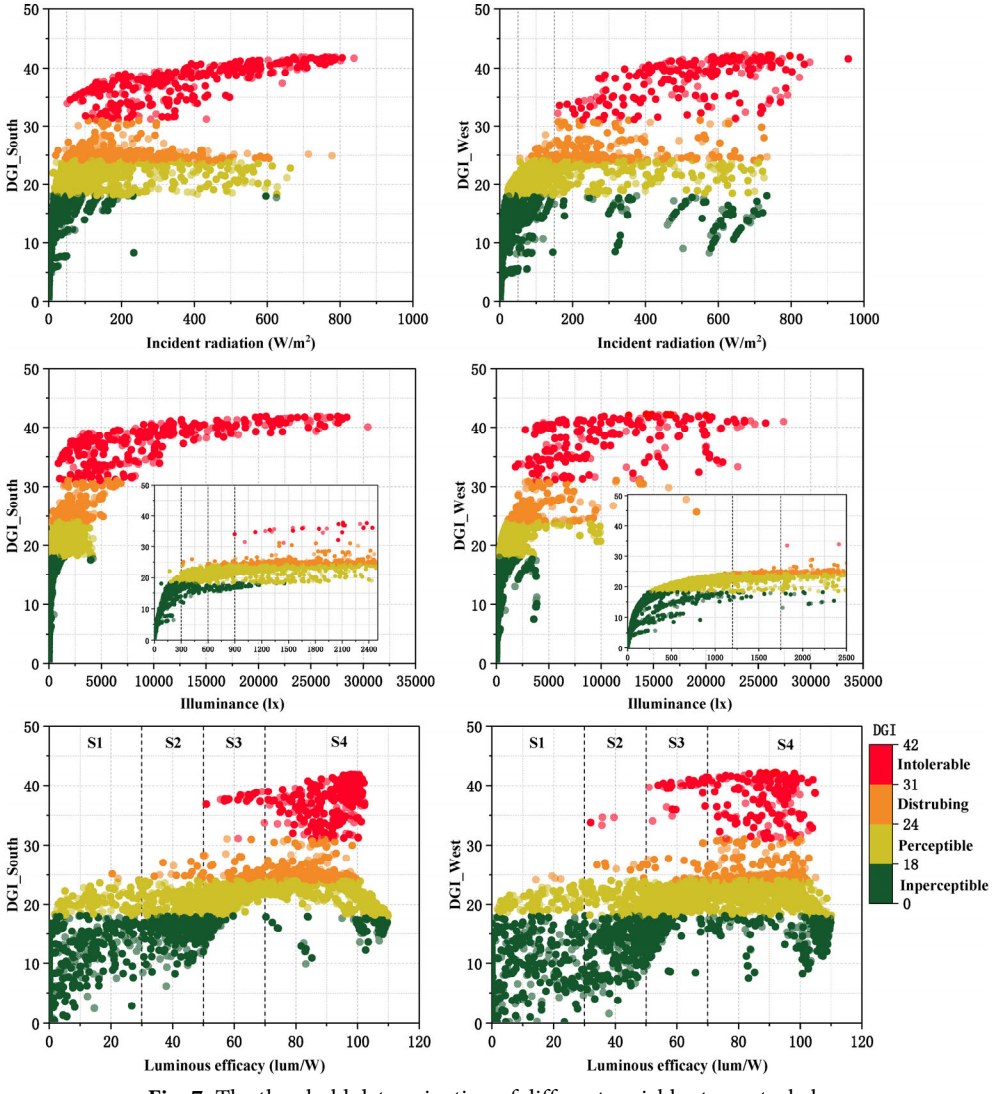

Fig. 7 The threshold determination of different variables to control glare

Table 4 Various rule-based control strategies used in this study

Ctrl strategies	Orientations		Conditions	Tint states
CtrlRad	South	If	Radiation < 50	Set state = S1
		Else if	Radiation < 100	Set state = S2
		Else		Set state = S4
	West	If	Radiation < 50	Set state = S1
		Else if	Radiation < 100	Set state = S2
		Else if	Radiation < 150	Set state = S3
		Else		Set state = S4
CtrlIll	South	If	Illuminance < 300	Set state = S1
		Else if	Illuminance < 600	Set state = S2
		Else if	Illuminance < 900	Set state = S3
		Else		Set state = S4
	West	If	Illuminance < 250	Set state = S1
		Else if	Illuminance < 1200	Set state = S2
		Else if	Illuminance < 1750	Set state = S3
		Else		Set state = S4
CtrlEff	South and west	If	Efficacy < 30	Set state = S1
		Else if	Efficacy < 50	Set state = S2
		Else if	Efficacy < 70	Set state = S3
		Else		Set state = S4
CtrlHeat	East	If	Heat flow < 50	Set state = S1
		Else if	Heat flow < 150	Set state = S2
		Else		Set state = S3
	South	IF	Heat flow < 25	Set state = S1
		Else if	Heat flow < 50	Set state = S2
		Else		Set state = S3
	West	If	Heat flow < 100	Set state = S1
		Else if	Heat flow < 150	Set state = S2
		Else		Set state = S3
	North	If	Heat flow < 40	Set state = S1
		Else		Set state = S2

of the ATPV window. The first three strategies were only applied to the south- and west-facing windows and the CtrlHeat was used for the all four orientations. It is seen from Table 4 that the same strategy has different control rules for different orientations, and these rules were achieved through an embedded program in EnergyPlus, the energy management system (EMS), by adopting the ERL (EnergyPlus runtime language). Specifically, the ATPV window was treated as the actuator controlled by the control algorithm designed with the EMS based on different sensors (decision variables).

2.5 Evaluation metrics

The performance of the ATPV window under different control strategies was evaluated in three aspects: (1) energy performance considering heating, cooling, artificial lighting, and power generation, (2) occupants' comfort including thermal and visual comfort, and (3) utility grid friendliness. The energy performance was evaluated through the net energy consumption. The occupants' thermal and visual comfort was evaluated through PMV (predict mean vote) and daylight glare index (DGI) indicators, respectively. The utility grid friendliness was characterized by the hourly net-zero energy potential (R_{net}), a higher R_{net} means that the building is less dependent on the utility grid, in other words, less of a burden on the grid. In addition

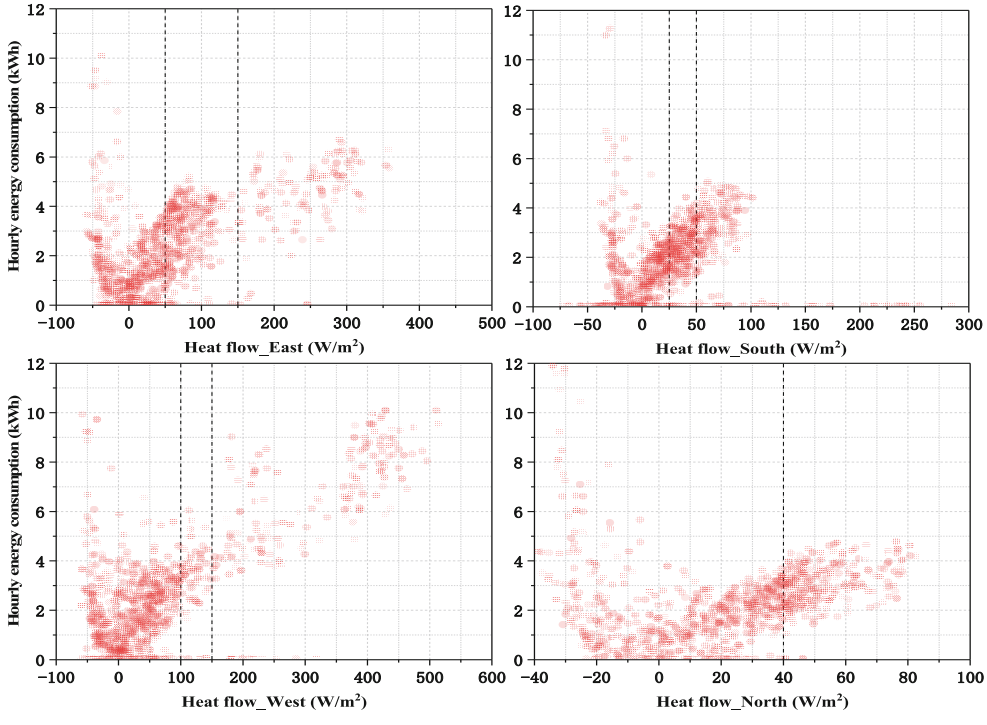

Fig. 8 The threshold determination of heat flow control

to evaluating the influence of the control strategies on different performances, the comprehensive performance of the ATPV window under different control strategies was analyzed considering the three aspects above. Then, the control strategy with the highest score of the comprehensive performance was considered as the optimal strategy in this study. All the evaluation metrics used in this study are listed in Table 5.

3 Results and discussions

3.1 Occupants' comfort

3.1.1 *Visual comfort*

Figure 9 depicts hourly DGI of south- and west-facing ATPV windows under different controls on sunny winter (Jan. 21st) and summer days (Jul. 15th). The DGI of the south-facing window on Jan. 21st is shown in Figure 9 (a), it is seen that the Low-E window and the ATPV window with bleached state result in similar visual comfort because they have closely static transmittance, while the DGI of the ATPV window under different control strategies are in different degrees. Specifically, the CtrlRad and CtrlEff strategies are the most effective strategies for glare protection, CtrlHeat strategy performs worst and followed by the CtrlIll strategy. This is because that the solar beam radiation and the beam solar radiation luminous efficacy have the highest correlation with indoor glare. As for the west-facing window on Jan. 21st, the CtrlEff strategy stands out among the four control strategies since most of the hourly DGI falls into the imperceptible bin. The CtrlIll and CtrlHeat strategies have almost the same impact on the DGI for the west-facing window. As for summer sunny days, both the DGI for south- and west-facing windows are lower than that on winter sunny days due to the less incident solar radiation. In summary, the CtrlRad and CtrlEff strategies perform similarly for the south-facing window, but the CtrlEff strategy is better than the CtrlRad strategy for the west-facing window.

Figure 10 depicts the hourly DGI distribution of different windows in south and west orientations. It is seen that the majority of DGIs for the south- and west-facing Low-E windows exceed the threshold of imperceptible glare (<18) due to the static high transmittance. All four control strategies of the ATPV window are capable of reducing glare with dynamic transmittance. For south-facing ATPV windows with CtrlRad and CtrlEff strategies, the percentage of DGI less than 18 is higher than 75%. For west-facing ATPV windows, the CtrlEff strategy is more effective than CtrlRad strategy because the vast majority of DGIs are below 18 with the CtrlEff strategy.

Figure 11 shows the year-round percentage of glare under different control strategies. As for south-facing window, it is seen that the imperceptible DGI percentages of Low-E window and ATPV window with bleached state are only 22% and 24%, while the intolerable DGI percentage is up to 12% for both. By employing CtrlRad strategy, CtrlIll strategy, CtrlEff Strategy, and CtrlHeat strategy for south-facing ATPV window, the imperceptible DGI percentages of ATPV window increase to 85%, 43%, 83%, and 37%, respectively. Besides, the percentages of intolerable glare can be reduced by 90.9%, 34.1%, 86.9%, and 13.3%. As for west-facing window, the imperceptible DGI percentages of Low-E window and ATPV window with bleached state are 30% and 33%, and by adopting the strategies above, the corresponding

Table 5 evaluation metrics used in this study

Aspects	Metrics	Formulas		Goals
Energy performance	Net-energy	Net-energy $= \sum_{i=1}^{4015}\left[\text{if}\left(E_{\text{light},i}+E_{\text{cooling},i}+E_{\text{heating},i}-E_{\text{pv},i}\right)>0\right]$		Min
Occupant comfort	DGI	Imperceptible:	DGI <18	$\text{Max\_DGI}_{<18}$
		Perceptible:	DGI 18–24	
		Disturbing:	DGI 24–31	
		Intolerable:	DGI >31	
	PMV	Comfort:	PMV $\in$ [−0.5,0.5]	$\text{Max\_PMV}_{[-0.5,0.5]}$
		Slight cool/warm:	PMV $\in$ [−1,1]	
		Cool/warm:	PMV $\in$ [−2,2]	
		Cold/hot:	PMV $\in$ [−3,3]	
Grid friendliness	R_{net}	$R_{\text{net}}=\frac{\sum_{i=1}^{4015}E_i}{4015}$ $E_i=\begin{cases}1 & \text{if Net-energy}>0\\ 0 & \text{if Net-energy}<0\end{cases}$		Max

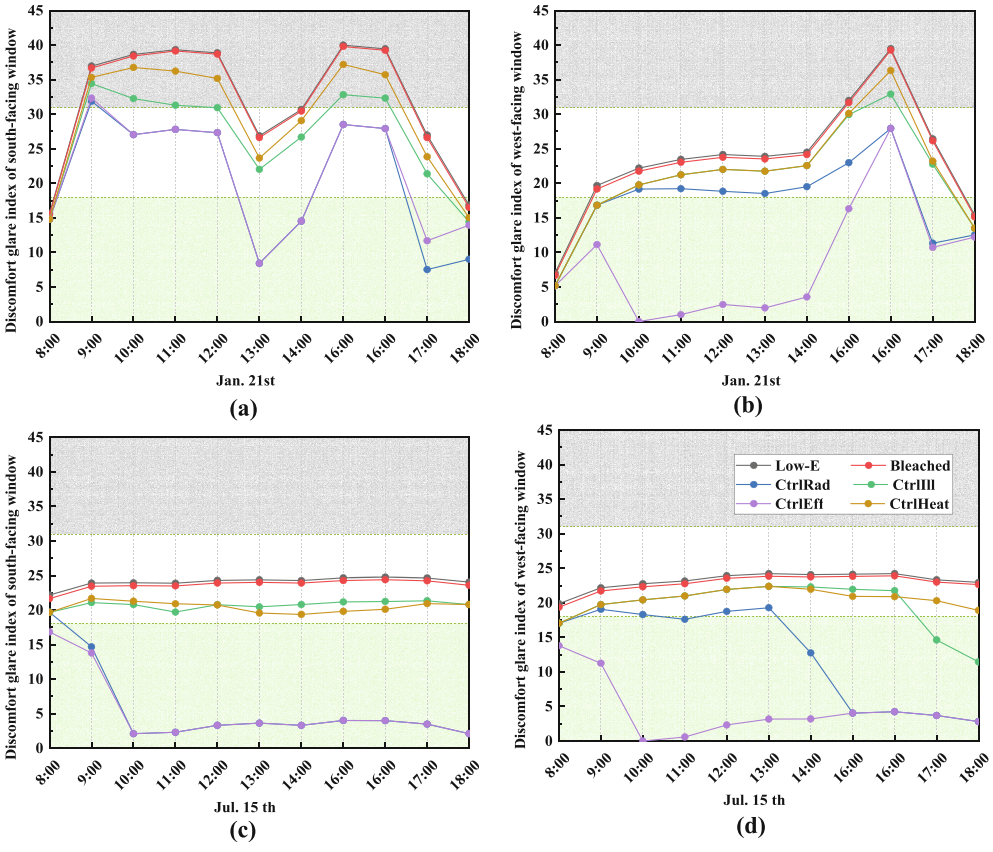

Fig. 9 Hourly discomfort glare index of south- and west-facing PVEC window on Jan. 21st and Jul. 15th

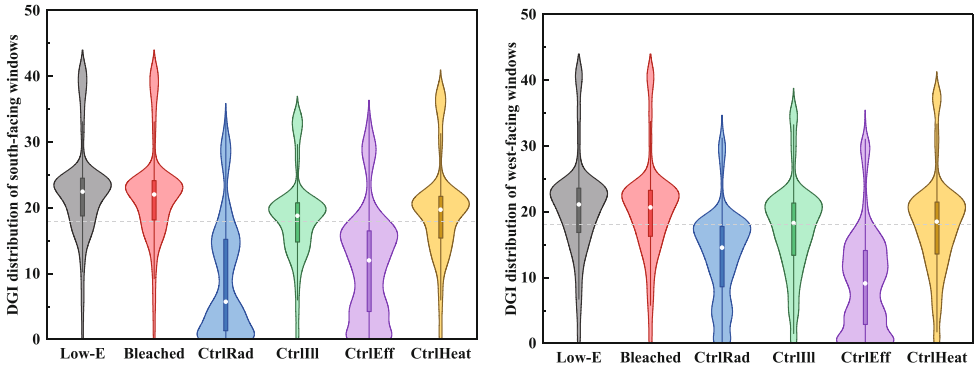

Fig. 10 Hourly DGI distribution of south- and west-facing windows

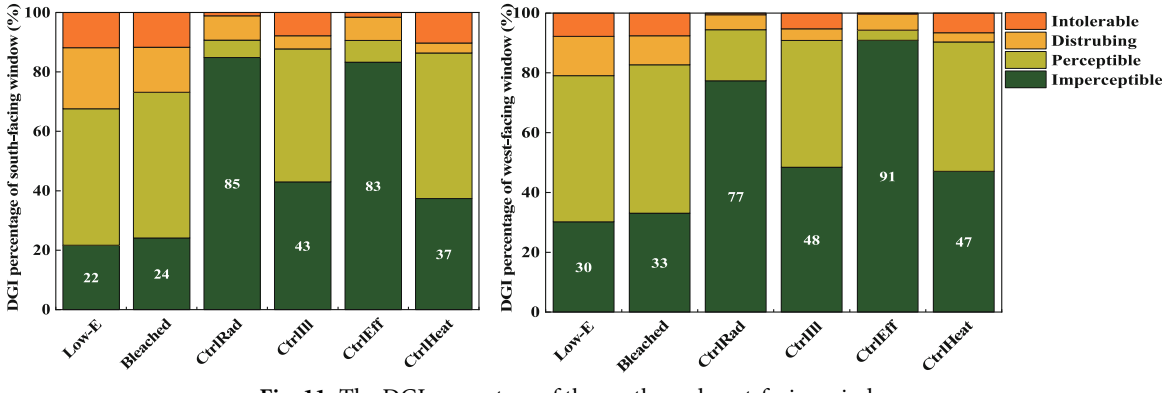

Fig. 11 The DGI percentage of the south- and west-facing windows

imperceptible DGI percentages rise to 77%, 48%, 91%, and 47%, and the reductions of intolerable DGI percentage are 92.3%, 32.1%, 94.9%, and 15.1%, respectively. Therefore, from the point of view of glare avoidance alone, CtrlRad and CtrlEff strategies are the optimal ones for the south- and west-facing windows with the largest glare reductions.

3.1.2 Thermal comfort

Figure 12 shows the hourly PMV of the south-facing Low-E window and ATPV window under the CtrlRad strategy. It is seen that for cooling season (from June 25th to August 23rd) and non-air-conditioned season, ATPV window can effectively alleviate the overheating problem since it can avoid excessive solar radiation entering the room by reducing its transmittance. For heating season (from December 26th to February 11th), the ATPV window has more serious problems with subcooling. This is because the beneficial indoor heat gain is reduced when avoiding glare by dimming the window transmittance, but the indoor heat gain in heating season is valuable for enhancing thermal comfort.

Figure 13 depicts the number of thermal comfort hours with different control strategies in four orientations. In general, the thermal comfort performance of ATPV windows with/without control strategies is better than that of the Low-E window except for the north orientation. This is because that the north-facing window receives least solar radiation, while the ATPV window lowers the transmitted solar radiation and causes the over-cooling problem. As for south-, west-, and east-facing ATPV windows with different control strategies, the thermal comfort hours increase by around 5%, 2% and 1%, respectively, on average compared with the Low-E window. Besides, it is noting that the impact of the control strategy on the thermal performance of the ATPV window is more obvious for the south-facing window, and the CtrlRad and CtrlEff strategies yield the best thermal comfort. This is because the south-facing window receives the largest solar radiation, which may lead to an overheating problem, and the CtrlRad and CtrlEff strategies are more effective to modulate the transmitted solar heat gain by changing tint states. Therefore, from the perspective of enhancing thermal comfort, CtrlRad and CtrlEff strategies are recommended for the south-facing window.

3.2 Net energy consumption

This section analyzed the hourly net energy consumption of the ATPV window under different controls on typical winter and summer days. Net energy consumption greater than 0 indicates that the PV generation is insufficient to meet the energy consumption. And net energy consumption less than 0 means that there is a surplus of electricity when the PV generation has met the electricity consumption at that moment. Figure 14 depicts the hourly net energy consumption of the ATPV window facing different orientations on a winter day (Jan. 21st). It is seen that the energy consumption of the Low-E window remains constant at certain times of the day, for example, from

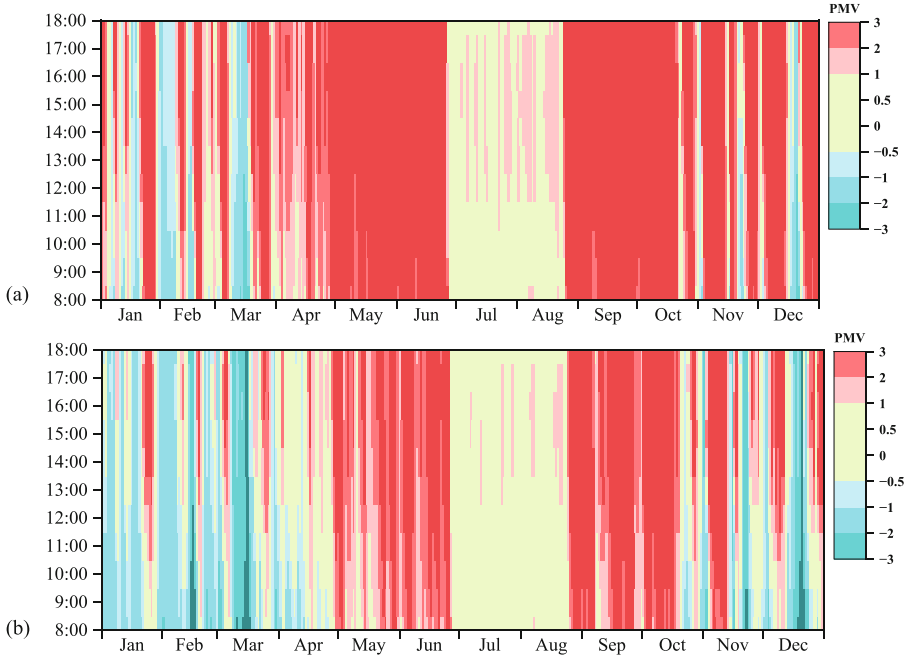

Fig. 12 Year-round hourly thermal comfort distribution of south-facing windows (a) Low-E window, and (b) ATPV window under CtrlRad control

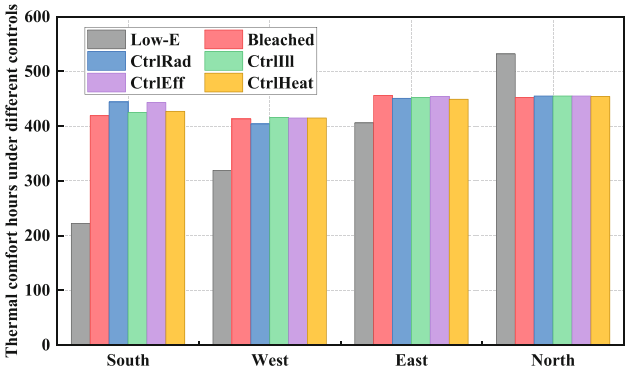

Fig. 13 Thermal comfort with ATPV windows under different controls

9:00 to 17:00 of the south-facing window. This is because the solar heat gain at this time can offset the heat loss caused by the temperature difference and the transmitted daylight can meet the minimum illumination requirements of the work plane, the load only contains personnel load and equipment load which do not vary with outdoor conditions during the day. Comparing the energy consumption of the ATPV windows with different controls, it is seen that the hourly energy consumption of the east- and north-facing ATPV windows do not change distinctly with different control strategies. While for the south- and west-facing ATPV windows, it is seen that the hourly energy consumption of the ATPV window varies with different control strategies, and the CtrlRad and CtrlEff strategies perform worse than others since they yield less power generation. Comparing the hourly energy consumption of the Low-E window and the ATPV window, it is seen that the ATPV window has surplus electricity during the time when solar radiation is abundant in each orientation.

Figure 15 depicts the hourly net energy consumption of the ATPV window facing different orientations on a summer day (Jul. 15th). It is seen that the hourly energy consumption of the south-facing ATPV window varies with different controls and the ATPV window with the CtrlHeat strategy performs the best due to the largest power generation. The power generations of the south-facing ATPV window with the CtrlRad and CtrlEff strategies are less than the other controls since the ATPV window with these two controls consumes more lighting energy when lowering the transmittance to reduce discomfort glare. As for the west-facing ATPV, the window with the CtrlRad strategy performs better than with the CtrlEff strategy, and the other control strategies have a similar performance compared with the south-facing window. There is little variation among the control strategies for the east- and north-facing windows because the east-facing ATPV is not controlled for glare protection, and the incident solar radiation does not vary much throughout the day.

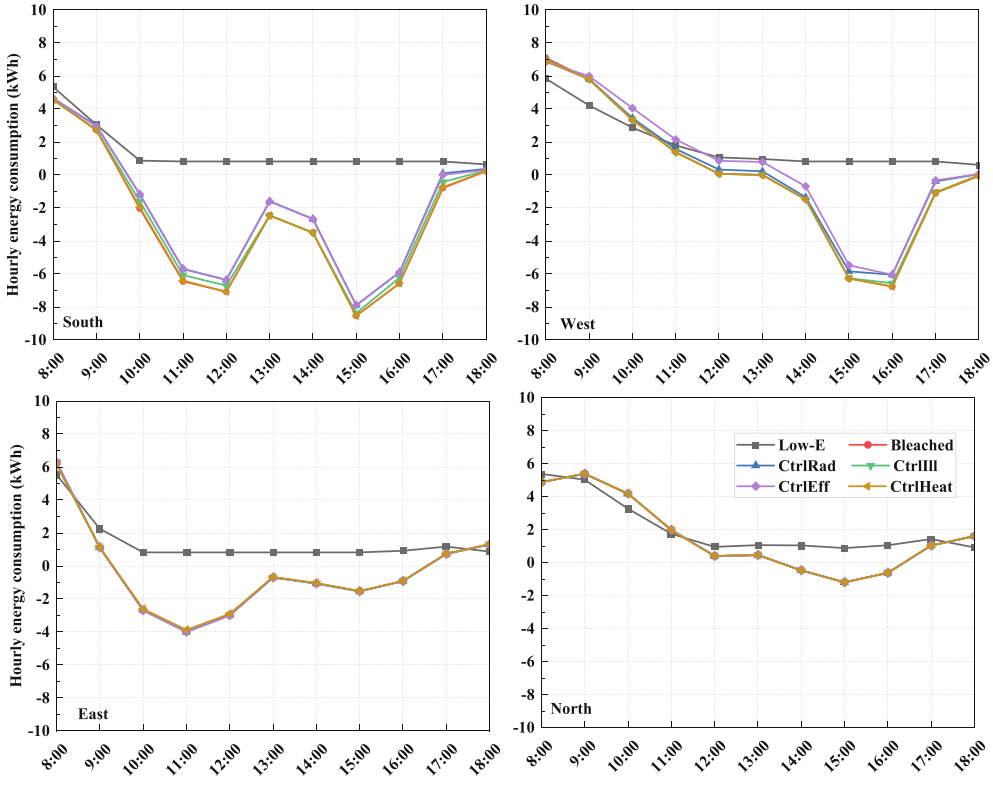

Fig. 14 Hourly energy consumption of different windows on Jan. 21st

To further elaborate on the benefits of ATPV windows, we analyzed the impact of ATPV windows on building cooling, heating and lighting energy consumption separately, as shown in Figure 16. It is seen that the west-facing windows consume the largest cooling energy, followed by the east-facing windows and the south-facing windows, while the north-facing windows have the lowest cooling energy consumption. The difference of cooling energy consumption between different orientations is due to the different incident solar radiations and different control effects of each control strategy for each orientation. North-facing windows receive the least amount of solar radiation and therefore the lowest cooling load was caused by the windows. Though the south-facing windows receive more solar radiation, the control strategy proposed in this study can effectively modulate the solar radiation entering the room, thus, the cooling energy consumption of the south-facing window is lower than the west- and east-facing

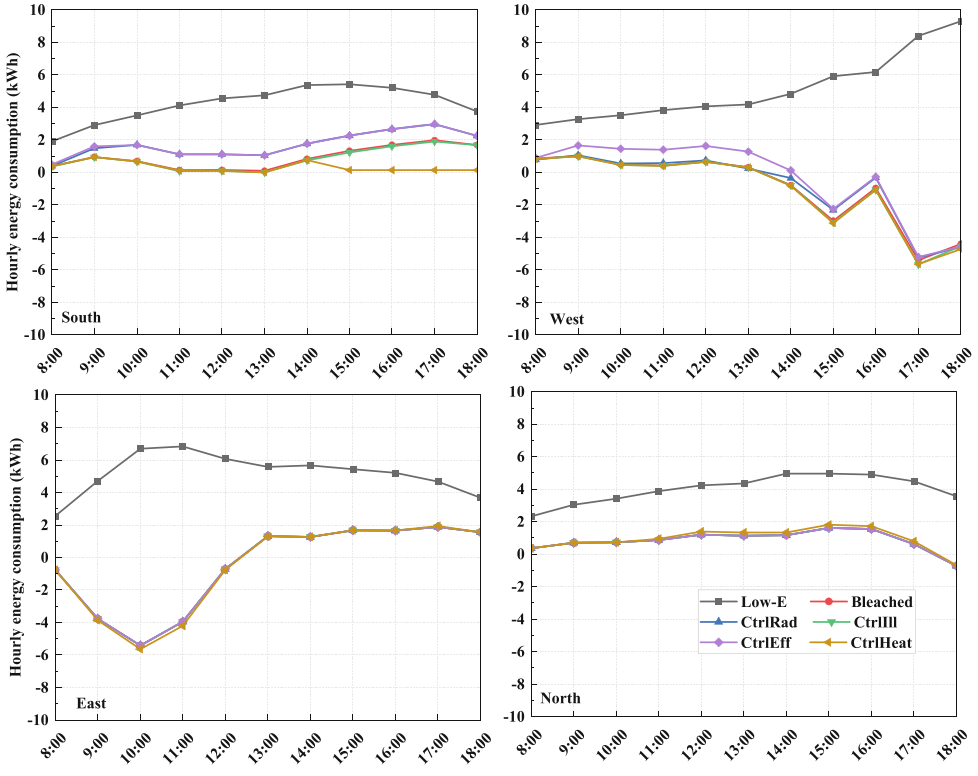

Fig. 15 Hourly energy consumption of different windows on Jul. 15th

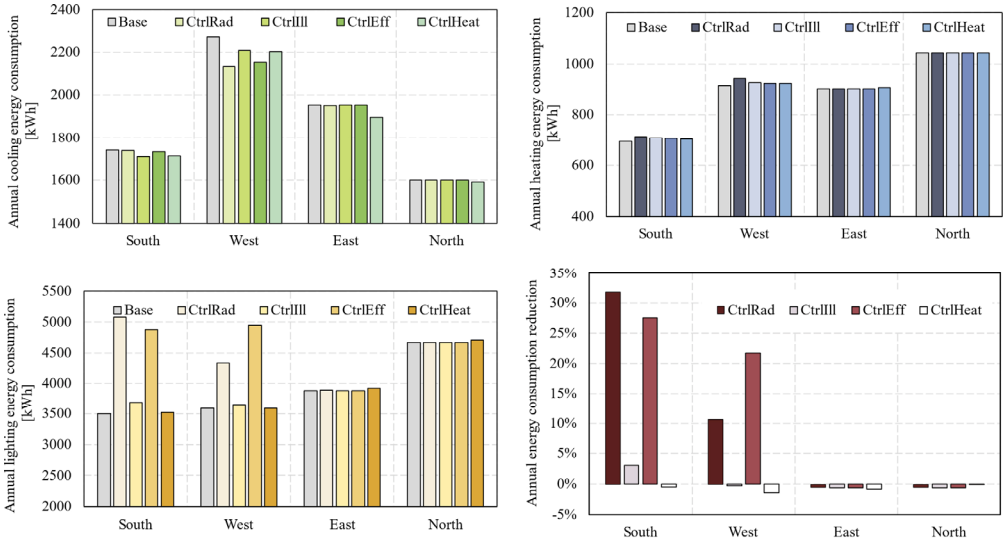

Fig. 16 Cooling, heating and lighting energy consumption of Low-E window and ATPV window under different control strategies

windows. As for heating energy consumption, it is noting that the heating energy consumption of the north-facing windows is the highest due to the least solar heat gain. The heating energy consumption of the south-facing window is the lowest since the south-facing window receives more beneficial solar radiation. The lighting energy consumption of the ATPV windows under different control strategies is more pronounced than the cooling and heating energy consumption. It is seen that the lighting energy consumption of the south- and west-facing windows under the CtrlRad and CtrlEff strategies is significantly larger than the other control strategies, and is almost twice than the lighting energy consumption of Low-E window. A comprehensive consideration of cooling, heating and lighting energy consumption reveals that the south-facing ATPV window under the CtrlRad strategy reduces 32% energy consumption and the total energy consumption of the west-facing ATPV window under the CtrlEff strategy decreases by 22%, when compared to the Low-E window.

It is seen from Figure 17(a) that the photovoltaic power generation of ATPV windows of different orientations are able to meet the annual energy consumption of the building in total, and the net PV power generations (total photovoltaic power generation minus total building energy consumption) in the south and west orientations are more than 4,000 kWh. This is because that the south and west ATPV windows receive the most solar radiation and generate more electricity, as shown in Figure 17(b). It is seen that the south-facing ATPV window generates the most electricity from January to March, and from October to December, the west-facing ATPV window generates the most electricity from April to September, and the north-facing window consistently generate the least electricity. However, due to the time mismatch between PV generation and building energy consumption, some of the electricity still needs to be taken from the utility grid to meet the building energy demand (net energy consumption). The annual net energy consumption of the Low-E window and ATPV window with different controls is shown in Figure 17(c). The ATPV window can decrease the net energy consumption significantly compared to the Low-E window with the average reductions of 58.7%, 65.7%, 64.1%, and 53.8% for the south, west, east and north orientations, respectively. More specifically, the energy savings of the ATPV window vary with the control strategies for the south and west orientations, and the ATPV window with the CtrlHeat strategy has the largest reductions of energy consumption. For the south-facing window, the window energy savings under the CtrlRad strategy is minimal at 53.8%, and for the west-facing window, the smallest reduction of energy consumption is 61.6% with the CtrlEff strategy. In general, the ATPV window has the greatest energy-saving potential

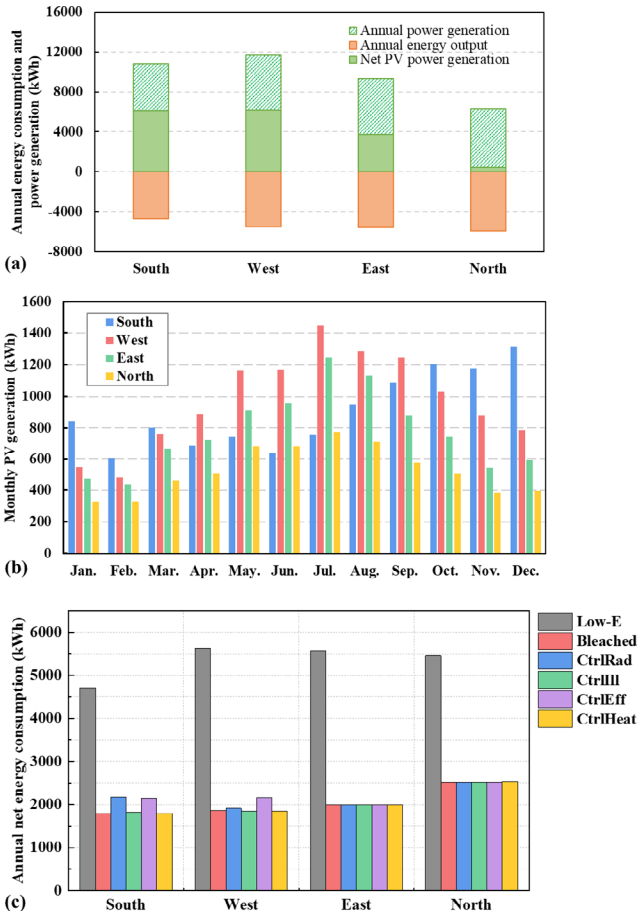

Fig. 17 (a) Annual PV power generation and energy consumption, (b) monthly PV power generation, and (c) annual net energy consumption of ATPV window with different controls

due to its power generation ability and the radiation modulation capacity.

3.3 Ratio of net-zero energy hours

Figure 18 depicts the ratio of net-zero energy hours (R_{net}) of ATPV windows facing different orientations during the daytime. For the east- and north-facing windows, the R_{net} of different rule-based controls is almost the same. This is because they have no glare protection demand, and the CtrlHeat strategy mainly influences the air conditioning energy consumption rather than the lighting energy consumption, which accounts for a large portion of the total energy consumption of the large-glazed perimeter office zone. It is seen that the highest zero-energy rate is about 78% occurred at around 11:00 since the east-facing window receives more solar radiation in the morning, and then the ratio gradually decreases as time goes on. The north-facing ATPV window receives the least solar radiation among the four orientations, therefore, the highest net-zero energy rate for north-facing windows is only about 70%,

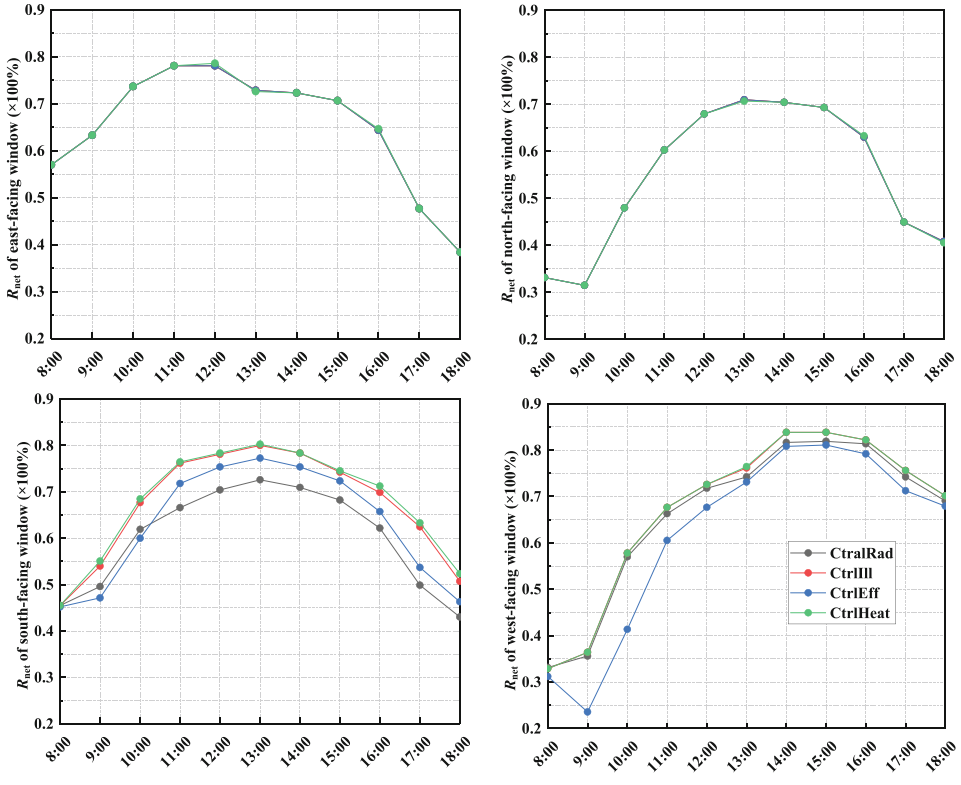

Fig. 18 Ratio of net-zero energy hours of ATPV window facing four orientations

occurring at around 13:00. It is worth noting that there is a significant difference in the R_{net} of south- and west-facing windows under different control strategies. For south- and west-facing windows, the highest R_{net}'s are both achieved under the CtrlHeat strategy, at 80% and 83.8%, respectively. However, the corresponding worst control strategies are CtrlRad and CtrlEff strategies. This is because the CtrlRad and CtrlEff are the most effective strategy for glare protection for south- and west-facing windows, respectively. The glare control will inevitably reduce the solar transmittance of the ATPV window, which increases the building's lighting energy consumption and thus reduce the R_{net}.

Figure 19 shows the annual net-zero energy ratio of the ATPV window under different control strategies in different orientations. In general, the north-facing window has the lowest R_{net}, which is mainly attributed to the fact that it receives less solar radiation than the others. The average R_{net} of the east- and north-facing windows are around 65.1% and 54.6%, respectively, while the R_{net} of the south-facing window varies from 60.1% to 67.6%, and for west-facing windows, the variation range is 61.6%–67.2%. The R_{net} reflects the grid-friendliness of the control strategy, a higher R_{net} implies less reliance on the utility grid. With this concern, the CtrlIll and CtrlHeat are recommended.

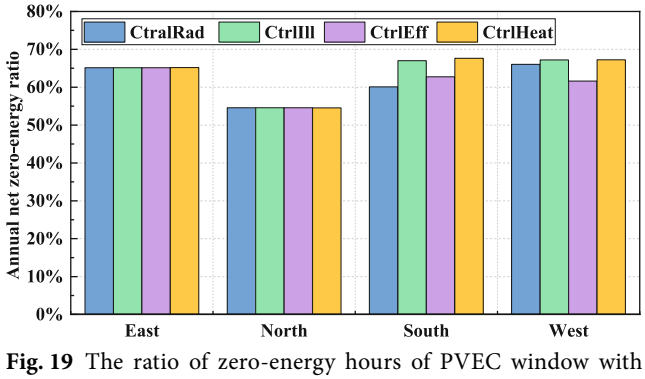

Fig. 19 The ratio of zero-energy hours of PVEC window with different controls

3.4 Comprehensive performance analysis

The investigation of the individual performance of various control strategies mentioned above reveals that the same strategy performs differently depending on the orientation. Furthermore, the identical control strategy has both good and bad effects on different performances. For east- and north-facing windows which do not has great glare protection demand, the optimal strategy can be selected for energy saving purpose. While for south- and west-facing windows, there is often a contradiction between avoiding glare and saving energy, thus, a comprehensive analysis needs to be considered. Figure 20 depicts the comprehensive performance of south- and west-facing windows under different control strategies considering net-zero energy ratio (R_{net}), glare reduction (R_g), thermal performance improvement (I_t), and

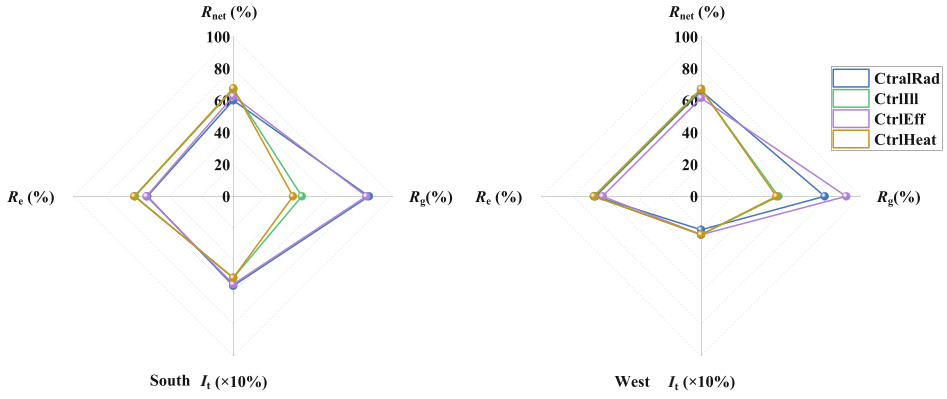

Fig. 20 Comprehensive performance of different control strategies for south- and west-facing windows

net energy reduction (R_e). It is seen clearly that the CtrlRad and CtrlEff strategies have the optimal performance for the south-facing window, and the CtrlEff strategy is the optimal control strategy for the west-facing window.

4 Conclusions

In this paper, an adjustable semi-transparent photovoltaic (ATPV) window was modeled based on measured data, and a novel rule-based control strategy taking the beam solar radiation luminous efficacy as the decision variable (CtrlEff) was proposed for the first time. To explore the feasibility and effectiveness of this strategy, several commonly used rule-based control strategies including the radiation control (CtrlRad), the illuminance control (CtrlIll), and the heat flow control (CtrlHeat) strategies were used as comparisons. A medium office building integrated with the ATPV window was modeled in EnergyPlus to simulate and evaluate its performance. The main conclusions of this study are drawn below:

(1) The ATPV window under the CtrlRad strategy minimizes the intolerable glare with a reduction of 90.9% for the south orientation, while for west orientations, the CtrlEff strategy performs the best with a glare reduction of 94.9%.

(2) Compared with the commonly used Low-E windows, the ATPV window can improve the thermal comfort hours by 5% and 2% for the south and west orientations, respectively.

(3) The ATPV window can decrease the net energy consumption by 58.7%, 65.7%, 64.1%, and 53.8% for the south, west, east, and north orientations, compared to the Low-E window.

(4) The annual net-zero energy ratio of the east- and north-facing ATPV windows are around 65.1% and 54.6%, respectively, while for the south- and west-facing windows, the ratios range from 60.1% to 67.6% and from 61.6% to 67.2% with different control strategies.

(5) The CtrlHeat strategy is recommended for the east- and north-facing ATPV windows, while the CtrlEff strategy is suggested for the south- and west-facing ATPV windows by comprehensively taking into account of the occupants' comfort, energy efficiency, and grid friendliness.

This study explored the comprehensive performance of the ATPV window under rule-based strategies. However, the proposed rule-based control strategies have not been optimized in this paper. In subsequent studies, an optimization model will be established to optimize the thresholds for each rule-based control to further exploit its potential in improving indoor comfort and reducing building energy consumption. Besides, a control platform, embedded with rule-based control policies, will be built for real-time control of ATPV windows.

Acknowledgements

This study has been supported by the National Natural Science Foundation of China (No. 51978252), the High-tech Industry Technology Innovation Leading Plan of Hunan Province (2020GK2076), the Science and Technology Innovation Program of Hunan Province (2020RC5003), the Hunan Province Innovation Development Program (2020RC4045), and the Hunan Province Key R&D Program (2021SK2045).

Declaration of competing interest

The authors have no competing interests to declare that are relevant to the content of this article.

Author contribution statement

Material preparation, data collection and analysis were performed by Yutong Tan and supervised by Jinqing Peng. The first draft of the manuscript was written by Yutong

Tan and all authors commented on previous versions of the manuscript. All authors read and approved the final manuscript.

References

Aburas M, Soebarto V, Williamson T, et al. (2019). Thermochromic smart window technologies for building application: A review. *Applied Energy*, 255: 113522.

Al-Qahtani SD, Binyaseen AM, Aljuhani E, et al. (2022). Production of smart nanocomposite for glass coating toward photochromic and long-persistent photoluminescent smart windows. *Ceramics International*, 48: 903–912.

Assimakopoulos MN, Tsangrassoulis A, Santamouris M, et al. (2007). Comparing the energy performance of an electrochromic window under various control strategies. *Building and Environment*, 42: 2829–2834.

Baldassarri C, Shehabi A, Asdrubali F, et al. (2016). Energy and emissions analysis of next generation electrochromic devices. *Solar Energy Materials and Solar Cells*, 156: 170–181.

Balta-Ozkan N, Yildirim J, Connor PM, et al. (2021). Energy transition at local level: Analyzing the role of peer effects and socio-economic factors on UK solar photovoltaic deployment. *Energy Policy*, 148: 112004.

Castillo MS, Liu X, Abd-AlHamid F, et al. (2022). Intelligent windows for electricity generation: A technologies review. *Building Simulation*, 15: 1747–1773.

Chen Y, Xiao Y, Zheng S, et al. (2018). Dynamic heat transfer model and applicability evaluation of aerogel glazing system in various climates of China. *Energy*, 163: 1115–1124.

Cheng C-Y, Chiang Y-J, Yu H-F, et al. (2021). Designing a hybrid type photoelectrochromic device with dual coloring modes for realizing ultrafast response/high optical contrast self-powered smart windows. *Nano Energy*, 90: 106575.

Dahanayake KC, Chow CL (2018). Comparing reduction of building cooling load through green roofs and green walls by EnergyPlus simulations. *Building Simulation*, 11: 421–434.

Deb SK, Lee S-H, Edwin Tracy C, et al. (2001). Stand-alone photovoltaic-powered electrochromic smart window. *Electrochimica Acta*, 46: 2125–2130.

Fang Y, Memon S, Peng J, Tyrer M, et al. (2020). Solar thermal performance of two innovative configurations of air-vacuum layered triple glazed windows. *Renewable Energy*, 150: 167–175.

Fathi S, Kavoosi A (2021). Effect of electrochromic windows on energy consumption of high-rise office buildings in different climate regions of Iran. *Solar Energy*, 223: 132–149.

Favoino F, Overend M, Jin Q (2015). The optimal thermo-optical properties and energy saving potential of adaptive glazing technologies. *Applied Energy*, 156: 1–15.

Fernandes LL, Lee ES, Ward G (2013). Lighting energy savings potential of split-pane electrochromic windows controlled for daylighting with visual comfort. *Energy and Buildings*, 61: 8–20.

Fiorito F, Cannavale A, Santamouris M (2020). Development, testing and evaluation of energy savings potentials of photovoltachromic windows in office buildings. A perspective study for Australian climates. *Solar Energy*, 205: 358–371.

Ganji Kheybari A, Steiner T, Liu S, et al. (2021). Controlling switchable electrochromic glazing for energy savings, visual comfort and thermal comfort: A model predictive control. *CivilEng*, 2: 1019–1053.

Ghosh A, Norton B, Mallick TK (2018). Influence of atmospheric clearness on PDLC switchable glazing transmission. *Energy and Buildings*, 172: 257–264.

Ghosh A, Norton B (2019). Optimization of PV powered SPD switchable glazing to minimise probability of loss of power supply. *Renewable Energy*, 131: 993–1001.

González J, Fiorito F (2015). Daylight design of office buildings: optimisation of external solar shadings by using combined simulation methods. *Buildings*, 5: 560–580.

Granqvist CG, Azens A, Heszler P, et al. (2007). Nanomaterials for benign indoor environments: Electrochromics for "smart windows", sensors for air quality, and photo-catalysts for air cleaning. *Solar Energy Materials and Solar Cells*, 91: 355–365.

Gugliermetti F, Bisegna F (2003). Visual and energy management of electrochromic windows in Mediterranean climate. *Building and Environment*, 38: 479–492.

Hong X, Shi F, Wang S, et al. (2021). Multi-objective optimization of thermochromic glazing based on daylight and energy performance evaluation. *Building Simulation*, 14: 1685–1695.

Hu S, Zhang Y, Yang Z, et al. (2022). Challenges and opportunities for carbon neutrality in China's building sector—Modelling and data. *Building Simulation*, 15: 1899–1921.

Huang L-M, Kung C-P, Hu C-W, et al. (2012). Tunable photovoltaic electrochromic device and module. *Solar Energy Materials and Solar Cells*, 107: 390–395.

Huang Y, Yang S, Aadmi M, et al. (2023). Numerical analysis on phase change progress and thermal performance of different roofs integrated with phase change material (PCM) in Moroccan semi-arid and Mediterranean climates. *Building Simulation*, 16: 69–85.

Jelle BP, Hynd A, Gustavsen A, et al. (2012). Fenestration of today and tomorrow: A state-of-the-art review and future research opportunities. *Solar Energy Materials and Solar Cells*, 96: 1–28.

Jonsson A, Roos A (2010). Evaluation of control strategies for different smart window combinations using computer simulations. *Solar Energy*, 84: 1–9.

Khatibi A, Hossein Jahangir M, Razi Astaraei F (2022). Energy and comfort evaluation of a novel hybrid control algorithm for smart electrochromic windows: A simulation study. *Solar Energy*, 241: 671–685.

Krarti M (2022). Energy performance of control strategies for smart glazed windows applied to office buildings. *Journal of Building Engineering*, 45: 103462.

Lee ES, Tavil A (2007). Energy and visual comfort performance of electrochromic windows with overhangs. *Building and Environment*, 42: 2439–2449.

Ling H, Wu J, Su F, et al. (2021). Automatic light-adjusting electrochromic device powered by perovskite solar cell. *Nature Communications*, 12: 1–8.

Ling H, Wu J, Su F, et al. (2022). High performance electrochromic supercapacitors powered by perovskite-solar-cell for real-time light energy flow control. *Chemical Engineering Journal*, 430: 133082.

Loonen R, Hensen J (2015). Smart windows with dynamic spectral selectivity—A scoping study. In: Proceedings of the 14th International IBPSA Building Simulation Conference, Hyderabad, India.

MOHURD (2012). GB 50033-2013. Standard for Daylighting Design of Buildings. Ministry of Housing and Urban-Rural Development of China. (in Chinese)

MOHURD (2015). GB 50189-2015. Design Standard for Energy Efficiency of Public Buildings. Ministry of Housing and Urban-Rural Development of China. (in Chinese)

MOHURD (2020). JGJ/T 67-2019. Standard for Design of Office Building. Ministry of Housing and Urban-Rural Development of China. (in Chinese)

MOHURD (2021). GB55015-2021. General Code for Energy Efficiency and Renewable Energy Application in Buildings. Ministry of Housing and Urban-Rural Development of China. (in Chinese)

Oh M, Park J, Roh S, et al. (2018). Deducing the optimal control method for electrochromic triple glazing through an integrated evaluation of building energy and daylight performance. *Energies*, 11: 2205.

Pal SK, Alanne K, Jokisalo J, et al. (2016). Energy performance and economic viability of advanced window technologies for a new Finnish townhouse concept. *Applied Energy*, 162: 11–20.

Piccolo A, Marino C, Nucara A, et al. (2018). Energy performance of an electrochromic switchable glazing: Experimental and computational assessments. *Energy and Buildings*, 165: 390–398.

Qiu C, Yi YK, Wang M, et al. (2020). Coupling an artificial neuron network daylighting model and building energy simulation for vacuum photovoltaic glazing. *Applied Energy*, 263: 114624.

Ritter V, Matschi C, Schwarz D (2015). Assessment of five control strategies of an adjustable glazing at three different climate zones. *Journal of Facade Design and Engineering*, 3: 129–141.

Scorpio M, Ciampi G, Rosato A, et al. (2020). Electric-driven windows for historical buildings retrofit: Energy and visual sensitivity analysis for different control logics. *Journal of Building Engineering*, 31: 101398.

Serale G, Fiorentini M, Capozzoli A, et al. (2018). Model predictive control (MPC) for enhancing building and HVAC system energy efficiency: Problem formulation, applications and opportunities. *Energies*, 11: 631.

Sullivan R, Lee ES, Papamichael K, et al. (1994). Effect of switching control strategies on the energy performance of electrochromic windows. In: Proceedings of SPIE 2255, Optical Materials Technology for Energy Efficiency and Solar Energy Conversion XIII, Freiburg, Germany.

Tan Y, Peng J, Luo Y, et al. (2022). Numerical heat transfer modeling and climate adaptation analysis of vacuum-photovoltaic glazing. *Applied Energy*, 312: 118747.

Tavares PF, Gaspar AR, Martins AG, et al. (2014). Evaluation of electrochromic windows impact in the energy performance of buildings in Mediterranean climates. *Energy Policy*, 67: 68–81.

Tavares P, Bernardo H, Gaspar A, et al. (2016). Control criteria of electrochromic glasses for energy savings in Mediterranean buildings refurbishment. *Solar Energy*, 134: 236–250.

Urbikain MK (2020). Energy efficient solutions for retrofitting a residential multi-storey building with vacuum insulation panels and low-E windows in two European climates. *Journal of Cleaner Production*, 269: 121459.

Wang J, Sheng S, He Z, et al. (2021). Self-powered flexible electrochromic smart window. *Nano Letters*, 21: 9976–9982.

Wu J-J, Hsieh M-D, Liao W, et al. (2009). Fast-switching photovoltachromic cells with tunable transmittance. *ACS Nano*, 3: 2297–2303.

Xia X, Ku Z, Zhou D, et al. (2016). Perovskite solar cell powered electrochromic batteries for smart windows. *Materials Horizons*, 3: 588–595.

Yao J, Zhu N (2012). Evaluation of indoor thermal environmental, energy and daylighting performance of thermotropic windows. *Building and Environment*, 49: 283–290.

Yik F, Bojić M (2006). Application of switchable glazing to high-rise residential buildings in Hong Kong. *Energy and Buildings*, 38: 463–471.

Zhang S, Hu W, Li D, et al. (2021). Energy efficiency optimization of PCM and aerogel-filled multiple glazing windows. *Energy*, 222: 119916.

Zhao D, Zhang G, Zhang X, et al. (2018). Optical properties of paraffin at temperature range from 40 to 80 °C. *Optik*, 157: 184–189.

Zhou Y, Fan F, Liu Y, et al. (2021). Unconventional smart windows: Materials, structures and designs. *Nano Energy*, 90: 106613.